Plasma Sources Sci. Technol. **20** (2011) 015007 (9pp) doi:10.1088/0963-0252/20/1/015007

Ambipolar ion acceleration in an expanding magnetic nozzle

Benjamin W Longmier[1], Edgar A Bering III[2], Mark D Carter[1], Leonard D Cassady[1], William J Chancery[1], Franklin R Chang Díaz[1], Tim W Glover[1], Noah Hershkowitz[3], Andrew V Ilin[1], Greg E McCaskill[1], Chris S Olsen[1] and Jared P Squire[1]

[1] Ad Astra Rocket Company, 141 W. Bay Area Blvd, Webster, TX, USA
[2] Department of Physics and Department of Electrical and Computer Engineering, University of Houston, 617 Science and Research Building 1, Houston, TX, USA
[3] Department of Engineering Physics, University of Wisconsin, 1500 Engineering Dr., Madison, WI, USA

Received 7 May 2010, in final form 4 November 2010
Published 7 January 2011
Online at stacks.iop.org/PSST/20/015007

Abstract
The helicon plasma stage in the Variable Specific Impulse Magnetoplasma Rocket (VASIMR®) VX-200i device was used to characterize an axial plasma potential profile within an expanding magnetic nozzle region of the laboratory based device. The ion acceleration mechanism is identified as an ambipolar electric field produced by an electron pressure gradient, resulting in a local axial ion speed of Mach 4 downstream of the magnetic nozzle. A 20 eV argon ion kinetic energy was measured in the helicon source, which had a peak magnetic field strength of 0.17 T. The helicon plasma source was operated with 25 mg s^{-1} argon propellant and 30 kW of RF power. The maximum measured values of plasma density and electron temperature within the exhaust plume were 1×10^{20} m^{-3} and 9 eV, respectively. The measured plasma density is nearly an order of magnitude larger than previously reported steady-state helicon plasma sources. The exhaust plume also exhibits a 95% to 100% ionization fraction. The size scale and spatial location of the plasma potential structure in the expanding magnetic nozzle region appear to follow the size scale and spatial location of the expanding magnetic field. The thickness of the potential structure was found to be 10^4 to 10^5 λ_{De} depending on the local electron temperature in the magnetic nozzle, many orders of magnitude larger than typical laboratory double layer structures. The background plasma density and neutral argon pressure were 10^{15} m^{-3} and 2×10^{-5} Torr, respectively, in a 150 m^3 vacuum chamber during operation of the helicon plasma source. The agreement between the measured plasma potential and plasma potential that was calculated from an ambipolar ion acceleration analysis over the bulk of the axial distance where the potential drop was located is a strong confirmation of the ambipolar acceleration process.

(Some figures in this article are in colour only in the electronic version)

1. Introduction

Single stage helicon sources and electron cyclotron resonance (ECR) plasma sources have previously been proposed as stand-alone electrodeless thrusters for spacecraft propulsion [1–27]. The concept takes advantage of a plasma potential step as a means to accelerate the escaping ions. Charge neutrality of the thruster/spacecraft system is maintained by a population of high energy electrons that overcome the plasma potential step to escape at the same rate as the ions. The plasma potential step is typically described as a current free double layer (CFDL), ambipolar diffusion/flow, a balance between electron pressure and magnetic pressure or some combination of these individual processes [8–34].

The presence of a plasma potential structure was observed during the helicon-only operation of the Variable Specific Impulse Magnetoplasma Rocket (VASIMR®) VX-200i, and is attributed to the generation of an ambipolar potential drop that results from an electron pressure gradient that occurs as the plasma escapes from the helicon source's magnetic

Figure 1. VASIMR® VX-200i prototype.

nozzle. A large downstream vacuum chamber size, >5 m, low background plasma density, $<10^{15}$ m^{-3}, and low background neutral pressure, $<2 \times 10^{-5}$ Torr, yielded unique and novel operating conditions.

It has been shown that the observed energy of ions emitted from double layer thrusters in a laboratory setting exhibits a direct correlation with the neutral gas background pressure [11–15, 25–27], which could actually be a result of a large population of electrons in the downstream plasma [29, 30, 32]. Charles *et al* show that the range of gas background pressures that corresponds to the largest potential step in a typical helicon thruster double layer is $\sim 2 \times 10^{-4}$ to 2×10^{-3} Torr for argon [20, 23, 35–37]. Double layer thruster operation in space will necessarily have a neutral background pressure many orders of magnitude lower than 10^{-4} Torr in the far plume region. More experiments are needed to resolve the existence of double layers generated by an expanding plasma source in a laboratory setting at background pressures below 10^{-4} and associated low background plasma densities. Hershkowitz *et al* [29, 30, 32] claim that the formation of a laboratory double layer may *require* a low density background population of electrons to flow upstream into the double layer plasma source or double layer thruster. The goal of the experiments presented in this paper is to expand on existing research performed by Charles [11–15, 21, 24, 27, 35, 36], Boswell [9, 11–15, 21, 27, 36], Lieberman [21, 23, 36], Chen [9, 22], Hershkowitz [29–32], Scime [26], Fruchtman [33, 34], Breizman [40, 41], Batishchev [10], Bengston [42], Gilland [8] and many others and explore the nature of ion acceleration in an expanding magnetic nozzle in a new parameter space.

Though nominal VASIMR® operation [38] includes a second stage to accelerate ions through single pass ion cyclotron heating (ICH), the second stage was turned off for the experiments presented in this paper.

2. VX-200i device and supporting hardware

The VASIMR® VX-200i, figure 1 with person for scale, came online in October 2008 and had a peak magnetic field strength of 0.17 T. The VX-200i helicon source used during this experiment campaign was driven by a variable RF power amplifier with a coupling efficiency of 95% that delivered up to 30 kW to the plasma column in these experiments. The coupling efficiency is defined as $\eta_{\text{coupling}} = R_{\text{plasma}}/(R_{\text{plasma}} + R_{\text{circuit}})$, where R_{plasma} is the resistance of the plasma and R_{circuit} is the resistance of the RF matching and transmission circuit. The RF generator used for the VX-200i helicon source was a custom built solid state Nautel Limited unit, model VX200-1, capable of delivering 40 kW near the industrial standard of 6.78 MHz. An argon gas flow rate of 25 mg s^{-1} was used during this experiment campaign. The magnetic field schematic for the VX-200i is shown in figure 2, where $z = 0$ m is defined as the location where the gradient of B becomes non-zero in the magnetic nozzle, i.e. the location where the magnetic field lines begin to expand. In figure 2, the magnetic field lines that follow the helicon core walls terminate in the exhaust section of the vacuum chamber at approximately $z = 4.5$ m. Figure 2 also shows the helicon coupler, but does not show the ICH coupler, as is typically used in a VASIMR® device. The helicon source internal plasma facing structure was electrically floating, as were all plasma facing components within the core of the VX-200i device. No external electric currents are imposed on the plasma. However, since the plasma facing components of the vacuum chamber were all grounded, through interconnected conductors, there was no effort made to prevent net current from flowing within the plasma.

The Ad Astra Rocket Company vacuum chamber is 4.2 m in diameter, 10 m long, with a total internal volume of 150 m^3, figure 3. The vacuum chamber is partitioned into two sections, a rocket section and an exhaust section. The rocket section, $z < 0.5$ m, contains the entire VX-200i device and stays at a space-like vacuum pressure in order to prevent arcing and glow discharges near the matching circuit components. The rocket section is sealed off from the downstream section and is pumped by a 1000 L s^{-1} cryopump. One cryopanel, with a pumping rate of 50 000 L s^{-1}, was used during this experiment campaign and produced a base pressure of 1.7×10^{-8} Torr in the exhaust section of the vacuum chamber. Also shown in figure 3 is a 2.5 m by 5 m translation stage that carries a suite of plasma diagnostics for plume characterization. The translation stage uses two independent ball screws and is driven by vacuum compatible stepper motors which yield a positional resolution of 0.5 mm. A vertical member mounted to the translation stage holds a mounting table. Each diagnostic is bolted directly to the mounting table for precise alignment and positioning on the translation stage. The central solid line in the center of figure 3 depicts the full axial range, $0\text{ m} \leqslant z \leqslant 5\text{ m}$, of plasma potential measurements taken for the data presented in this paper. The solid line extends into the VASIMR® VX-200i device, but does not penetrate the helicon source itself, and extends 5 m downstream into the expanding plume region of the vacuum chamber.

Measurements of the plasma potential in the rocket core and the plasma plume were made with a 1/4 inch diameter tungsten Langmuir probe with a guard ring, figure 4 and inset of figure 5.

The probe was swept in voltage from −40 V to +40 V through the entire range of ion saturation and electron saturation regions with a sweep rate of 80 Hz and a sampling rate of 40 kHz. Without RF compensation, the peak-to-peak voltage fluctuations on the Langmuir probe produced

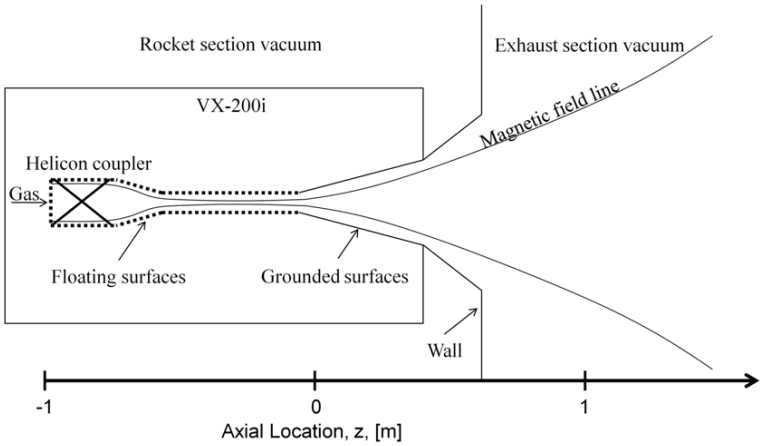

Figure 2. Schematic illustration of the VX-200i magnetic field and helicon coupler.

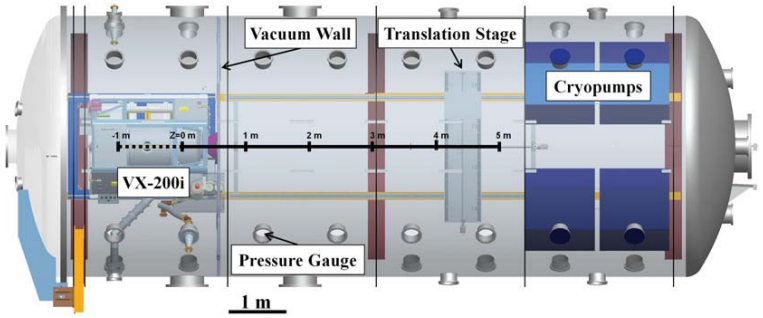

Figure 3. Schematic illustration of the Ad Astra Rocket Company vacuum chamber, overhead view.

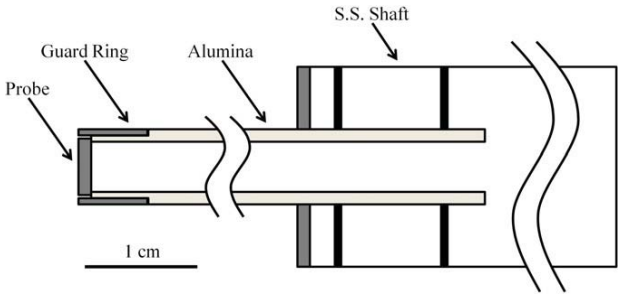

Figure 4. Schematic of the Langmuir probe with guard ring used to make measurements of V_p, T_e and N_e. The guard ring prevents radial sheath expansion.

± 0.2 V variations in the measured plasma potential, and ± 0.1 eV variations in the electron temperature. With RF compensation, the Langmuir probe measured peak to the peak voltage fluctuations that resulted in ± 0.1 V in measured plasma potential. RF compensation of the Langmuir probe was not used for the data presented in this paper since compensation often leads to shifts in measured plasma and floating potentials. Floating potential measurements were made with a high impedance oscilloscope from 1 Hz to 100 MHz. Fluctuations in the floating potential were observed to have a maximum peak-to-peak amplitude of 0.4 V at the driving frequency of the helicon plasma source, near the industrial standard 6.78 MHz. Measurements of the ion energy in the downstream section of the plume were made with a 4 grid retarding potential analyzer (RPA) [39]. Figure 5 shows a photograph of the argon exhaust plume produced by the helicon source from the VX-200i. The translation stage and plasma diagnostics can be seen in the background of the photograph. Plasma potential measurements were made with the Langmuir probe. The majority of the plasma potential drop occurs in the bright lobe in figure 5, as indicated by the superimposed graph.

3. Ambipolar ion acceleration

It has long been understood that the electron population in an expanding plasma could be responsible for establishing an electric field that contributes to ion acceleration in the form of a double layer or a more gradual ambipolar potential. The former phenomenon has been extensively studied by Boswell, Charles and others who have characterized the conditions under which laboratory double layers may form. These may be strongly dependent on the parameter space in which the experiment is carried out. The following experiments were performed to expand on the work done by Boswell and Charles *et al*, and in fact the original goal was to find and characterize a double layer within the VX-200i device.

It was observed that the helicon source in the VASIMR® VX-200i produces an acceleration of ions in the expanding magnetic nozzle region downstream of the helicon source. The measured plasma potential, V_p, electron temperature, T_e, and

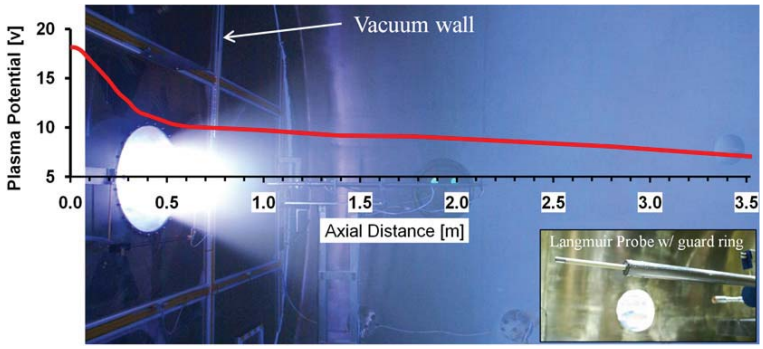

Figure 5. Photograph of the helicon exhaust plume with the translation stage and diagnostics in the background. The plasma potential drop (superimposed graph) occurs largely in the bright lobe. The lower right inset shows the Langmuir probe with guard ring on a 70 cm extension shaft.

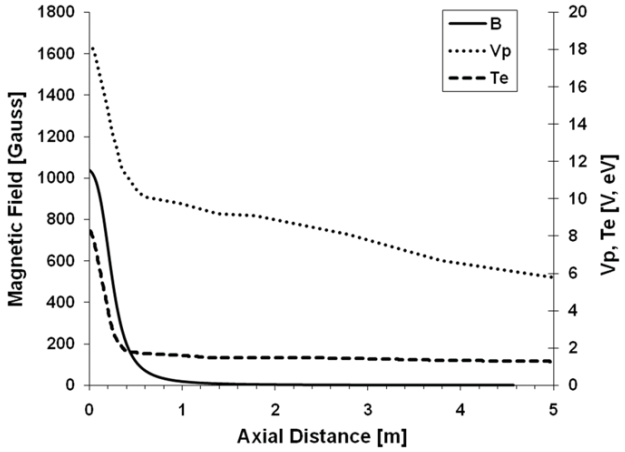

Figure 6. Measured plasma potential (V_p), electron temperature (T_e) and axial magnetic field strength (B) as a function of axial distance. Plasma potential and electron temperature measurements have error ± 0.5 V and ± 0.5 eV, respectively, for 0.25 m $< z <$ 0.75 m.

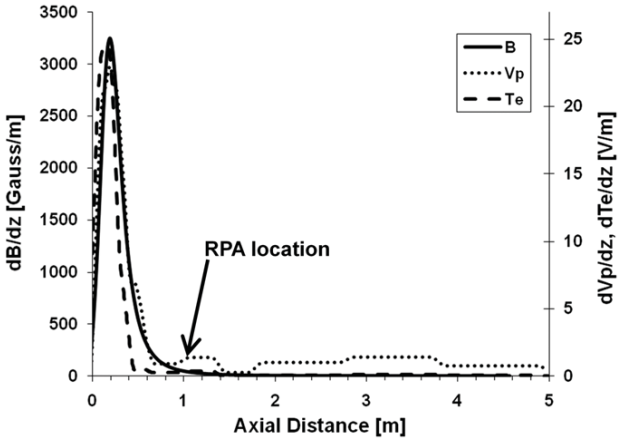

Figure 7. Spatial derivative of the measured plasma potential (V_p), electron temperature (T_e) and axial magnetic field strength (B) as a function of axial distance. Plasma potential and electron temperature measurements have an error ± 0.5 V for 0.25 m $< z <$ 0.75 m.

magnetic field strength, B, as a function of the axial distance in the exhaust plume of the VX-200i device are shown in figure 6. The high correlation between the measured axial V_p, T_e and B is more clearly seen if the spatial derivative is taken for V_p, T_e and B, as shown in figure 7. V_p and T_e were determined using standard Langmuir probe analysis with the guarded Langmuir probe described in section 2.

The thickness of the potential structure observed in the exhaust plume VX-200i device was found to be $10^5 \lambda_{De}$, many orders of magnitude larger than a double layer structure. A CFDL, as has been typically defined [11–15, 24], was not observed in the VX-200i device for the described operating conditions. The background plasma density throughout the experiments presented was below 10^{15} m^{-3}, with a neutral gas background pressure below 2×10^{-5} Torr. The argon charge exchange mean-free path was larger than 320 cm for all data presented. The ionization fraction of the plasma was 95% to 100%, as measured by the gas flow rate sensor and the Langmuir probe in ion saturation [43].

A total drop in the axial plasma potential, V_p, of 12 V was measured from location $z = 0$ m to $z = 5$ m. Plasma potential measurements were only made to an upstream location of $z = 0$ m. An additional increase in the magnetic field strength, up to 1700 G, at the magnetic choke ($z = -0.6$ m in figure 2) of the VX-200i device existed upstream of the $z = 0$ m location. Assuming ambipolar ion acceleration between -0.6 m $< z <$ 5 m, a resulting ion energy equal to 20 eV would be expected. RPA measurements revealed a mean argon ion energy in the downstream section of the VX-200i device of 22 $\pm$ 3 eV. Figure 8 is a representative graph of the I–V characteristic from the RPA (dashed) and the ion energy distribution function (solid) as a function of the RPA retarding potential. The RPA was located downstream of the magnetic nozzle, $z = 1.03$ m, and was able to measure the full ion energy from the VX-200i helicon source, figure 7.

Beginning at location $z = 0$ m, the magnetic field strength decreases monotonically, giving rise to an ambipolar flow of quasineutral plasma. In this monotonically decreasing region of interest, 0.25 m $< z <$ 0.75 m, the plasma density scales with the decreasing magnetic field such that $\nabla B \propto \nabla n_e$, as shown in figure 9. At axial distances $z >$ 1 m the electron density data were constant. Others have previously observed similar ion acceleration results from an expanding plasma along a magnetic nozzle [22, 44].

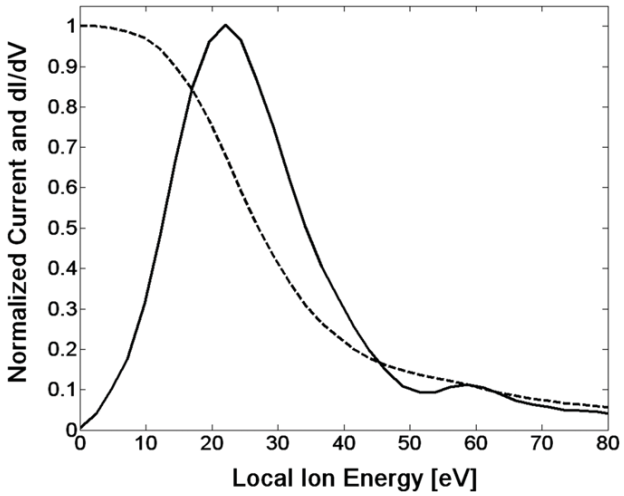

Figure 8. Normalized RPA I–V characteristic (dashed) and normalized ion energy distribution function (solid).

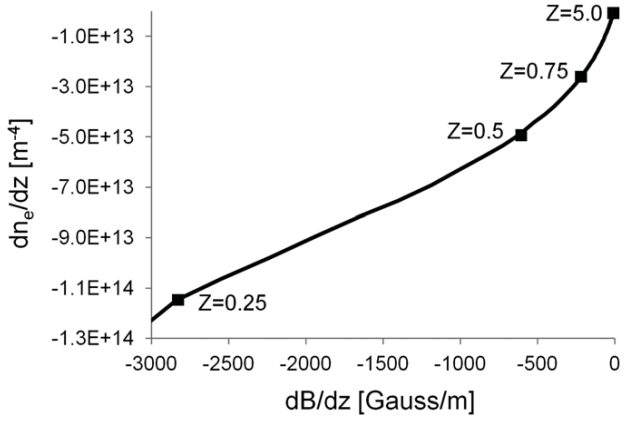

Figure 9. $\mathrm{d}n_\mathrm{e}/\mathrm{d}z$ versus $\mathrm{d}B/\mathrm{d}z$ for increasing axial distance.

4. Discussion

These data raise two major questions that one needs to understand in some detail. First, this work began with the expectation that the study would focus on the properties of CFDLs in a new regime. The absence of CFDLs was a surprise that raises the question of the physics responsible for preventing CFDLs from occurring. Second, what was observed instead was a macroscopic parallel electric field over a region that was thousands of Debye lengths in extent. In a plasma, parallel electric fields are somewhat unexpected. This observation raises the question of the physics responsible for producing and sustaining the parallel field.

4.1. The absence of CFDLs

This subsection will address the first question: what is the physics behind the absence of CFDLs? In a helicon plasma source the electron thermal velocity is much greater than the ion thermal velocity and as the electrons start to stream away from the helicon source in the magnetic nozzle, they create a potential step that acts to confine the total electron flux to that of the ion flux. The ions in the upstream section are consequently accelerated down the hill of this potential step, in this case to a velocity equal to $4.1 \pm 0.3 c_\mathrm{s}$, which was determined from an ion energy measurement from an RPA and a T_e measurement from a Langmuir probe, where $c_\mathrm{s} = (k_\mathrm{B} T_\mathrm{e}/m)^{1/2}$ at the location $z = 1.03$ m in the downstream end of the magnetic nozzle.

In the presence of a large population of isotropic electrons born in the downstream exhaust plume, the potential step will tend to accelerate these electrons back upstream toward the helicon source. It is possible that the presence of a large population of downstream electrons creates the commonly observed CFDL, and could explain why CFDLs are only observed for a finite range of downstream neutral pressure levels [30, 45]. In this experimental campaign, the downstream electron population was minimized as much as possible, usually held to a density less than $10^{15}\,\mathrm{m}^{-3}$, five orders of magnitude lower than the peak plasma density at $z = 0$ m, and an order of magnitude lower than previous experiments [30, 45].

4.2. Ambipolar acceleration and plasma transport in an expanding plasma nozzle

This subsection will address the second question: what is the physics responsible for producing and sustaining the parallel electric field. The most likely hypothesis is that the result is the signature of an ambipolar diffusion process. In this model, the electric field is the result of an electron pressure gradient. The available diagnostic data from the VX-200i exhaust plume are sufficient to validate this hypothesis by conducting a detailed quantitative investigation of the physics of plasma transport in the exhaust plume. Since the plasma in the VX-200i is strongly magnetized, one-dimensional field-aligned transport equations can be used [46]. Ambipolar flow in an expanding flow with isothermal electrons has been previously handled in general [47, 48], but here we cannot assume isothermal electrons since a strong electron temperature gradient was present. The model chosen assumes monoatomic ions with no internal degrees of freedom. Elastic ion–electron collisions and photoemission are not included. In this model, the field-aligned continuity equation for each species is

$$\frac{\partial}{\partial s}\left(\frac{m_s n_s u_s}{B}\right) = \frac{m_s S_s}{B} - L_s \frac{m_s n_s}{B}. \tag{1}$$

The field-aligned momentum equation for each species is

$$m_s n_s \frac{\partial u_s}{\partial t} + m_s n_s u_s \frac{\partial u_s}{\partial s} + \frac{\partial p_s}{\partial s} - m_s n_s g_\parallel - q_s n_s E_\parallel = \sum_t m_s n_s \bar{\nu}_{st}(u_{t\parallel} - u_s) \tag{2}$$

The field-aligned energy transport equation for each species is

$$\frac{3}{2}\frac{\partial}{\partial t}\left(\frac{p_s}{B}\right) + \frac{3}{2}\frac{\partial}{\partial s}\left(u_s \frac{p_s}{B}\right) + p_s \frac{\partial}{\partial s}\left(\frac{u_s}{B}\right) + \frac{\partial}{\partial s}\left(\frac{h_s}{B}\right) = \sum_t \frac{m_s n_s \bar{\nu}_{st}}{m_s + m_t}[3k(T_t - T_s) + m_t(\boldsymbol{u}_t - \boldsymbol{u}_s)^2] \tag{3}$$

where the variable s is the distance along the field line, subscripts s, t are particle species, m_s is mass, n_s is number

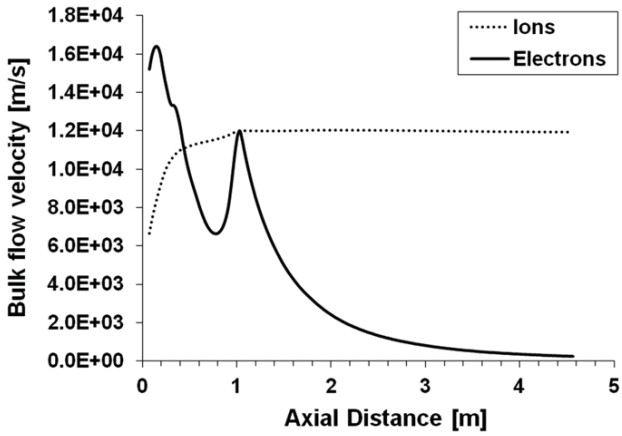

Figure 10. Calculated field-aligned electron (solid) and ion (dashed) bulk flow velocity as a function of axial distance in the plume region of the VX-200i.

density, u_s is the field-aligned component of the bulk flow velocity, B is the magnetic induction, h_s is the parallel component of the heat flow vector for species s, S_s is the ionization rate, L_s is the particle loss rate, t is the time, p_s is the scalar partial pressure, $g_\parallel$ is the component of the local gravitational acceleration parallel to B, $E_\parallel$ is the component of the electric field parallel to B, $\bar{\nu}_{st}$ is the momentum transfer collision rate between species s and t, k is Boltzmann's constant and T is temperature in kelvin.

The duration of each plasma shot was 12 s, which is long compared with all other time scales in the system, the plume is considered to be steady state for modeling purposes. The region of the plume that is being considered has no assumed sources of ionization. The mean-free path for charge exchange was ∼3 m, which indicates that the ion–neutral collision rate was low. Since L_s for either ions or electrons requires a 3-body interaction, the low rate of ion–neutral collisions and the corresponding low rate of ion–ion collisions indicates that recombination losses were negligible. The mean-free path for ionization was also several m in the exhaust region. Thus, it may be assumed that $L_s = \bar{\nu}_{st} = 0$ for both ions and electrons. Since we did not measure ion temperature as a function of z, this analysis will focus solely on the electrons. Thus, for electrons, these three equations reduce to

$$\frac{\partial}{\partial s}\left(\frac{m_e n_e u_e}{B}\right) = 0 \qquad \text{or} \qquad \frac{n_e u_e}{B} = \text{constant} \tag{4}$$

$$m_e n_e u_e \frac{\partial u_e}{\partial s} + \frac{\partial p_e}{\partial s} + e n_e E_\parallel = 0 \tag{5}$$

$$\frac{3}{2}\frac{\partial}{\partial s}\left(u_e \frac{p_e}{B}\right) + p_e \frac{\partial}{\partial s}\left(\frac{u_e}{B}\right) + \frac{\partial}{\partial s}\left(\frac{h_e}{B}\right) = 0 \tag{6}$$

The one-dimensional time-stationary continuity equation (equation (4)) was used to infer the field-aligned electron bulk flow velocity. The results appear as the solid curve in figure 10. The dashed curve shows the ion bulk flow velocity estimated from single particle dynamics, using the estimated plasma potential as discussed below and conservation of the first adiabatic invariant, and setting the ion velocity equal to the value of 12 km s^{-1} inferred from the RPA data at $z = 1.03$ m. The apparent exponential decay of the inferred electron velocity at axial distances $z > 1.05$ m is taken to indicate that the density data were dominated by noise in the downstream section, primarily owing to the unavailability of a large enough pre-amp feedback resistor during this campaign. The rest of the axial structure in the electron velocity occurs because the electron density profile does not exactly follow the decrease in the magnetic field shown in figure 9. The physics of this discrepancy is not well understood. Speculation suggests that this apparent structure results from shot-to-shot variations in overall plume density, since each axial point in the raw data represented a separate plasma shot. On the other hand, the inferred ion velocity conforms reasonably with expectations based on an ambipolar acceleration picture.

The lack of agreement between the ion and electron bulk flow velocities requires that a parallel current was flowing. A parallel current is, of course, an expected consequence of the parallel electric field.

The well-known Boltzmann relation is derived by integrating equation (5) under the assumption that the electrons were isothermal. An obvious first step in any analysis is to ignore the observed temperature gradient and see if solving the Boltzmann equation for an inferred electrostatic potential reproduces the measured potential. This procedure was tried. The resulting comparison (not shown) did not produce an inferred potential profile that was in agreement with observation, suggesting that the temperature gradient could not be ignored.

In principle, the one-dimensional time-stationary momentum equation (equation (5)) could be integrated to yield an independent estimate of the parallel electron bulk flow. In practice, the electron bulk flow is determined by the balance between the pressure gradient and electric field terms; which are both large and imprecisely known. Thus, the result of integrating the momentum equation is too uncertain to be meaningful. Instead, the electron velocity inferred from continuity was used with the electron temperature and pressure data to integrate the momentum equation and infer the plasma potential. The results of this integration are compared with measurements in figure 11. It should be noted that voltage limits of the sweeping power supply used for the guarded flux probe may have resulted in underestimates of the plasma potential for $z < 0.25$ m. Consequently, the integration was initiated at $z = 0.26$ m and taken in both directions. The measured and inferred curves are indistinguishable over the range $z = 0.25$ m to 0.75 m, which is the entirety of the range where both the density and potential data were reliable. At large z, density overestimates dominate the error budget, whereas at small z, the discrepancy between the two curves results from underestimates in the measured potential. The calculated potential in figure 11 was used to derive the ion velocity curve in figure 10. The agreement between the two curves in figure 11 over the bulk of the axial distance where the potential drop was located is a strong confirmation of the ambipolar acceleration picture.

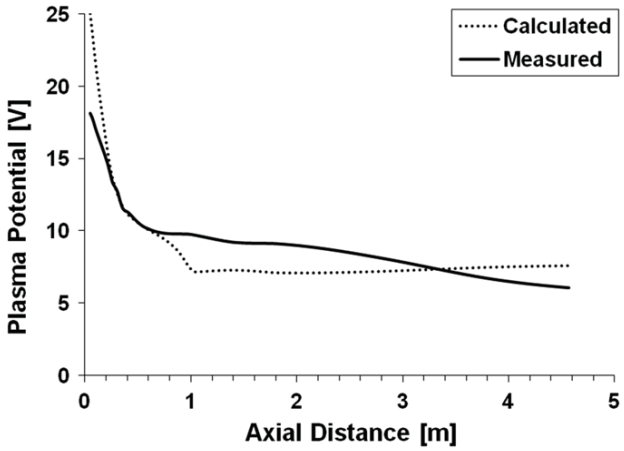

Figure 11. Calculated (dashed) and measured (solid) plasma potential as a function of axial distance in the plume region of the VX-200i.

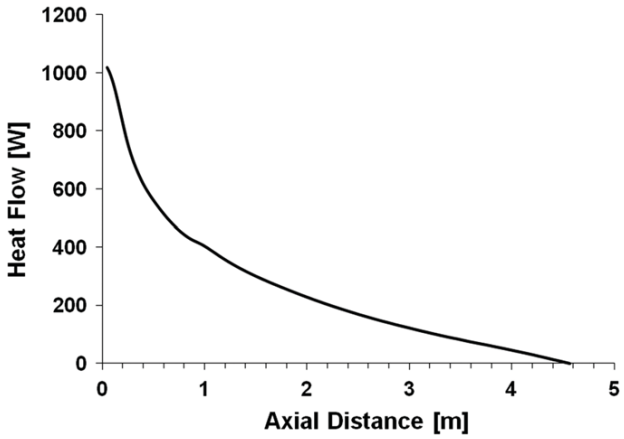

Figure 12. Heat flow as a function of axial distance from the helicon plasma source. A heat flow out of the nozzle is considered a positive heat flow.

The one-dimensional time-stationary energy equation (equation (6)) can be solved and then integrated to give the electron conduction heat flow into the plume region from the helicon source. The presence of an electron temperature gradient requires that there is a heat flow. As written, integration of the energy equation gives h/B. This result can be converted into an estimate of total heat flow from the helicon into the plume by multiplying by $A \cdot B(z = 0)$, where A is the area of the exhaust plume at the exit plane from the engine core. The results are shown in figure 12, and indicate that heat conduction from the helicon plasma source represents a heat-loss term of about 1 kW.

A limitation of this analysis is that it does not account for the observed electron temperature gradient. It demonstrates that the electron temperature gradient is consistent with the observed ambipolar electric field. However, it does not include an electron cooling mechanism. In fact, the required physics was taken out of the model in two steps. The glowing region of the plasma in figure 5 indicates what one of the cooling mechanisms was: electron–ion collisions producing radiation from bound–bound optical transitions. This cooling mechanism was omitted from the approximation to the collision integral that produced equation (3). The model completely neglected inelastic electron–ion collisions and the internal energy levels of the argon ions. We further assumed that the electron gas was collisionless.

If the ambipolar ion acceleration found in the helicon discharge of the helicon plasma source continues to scale proportional to ∇n_e, it is expected that a larger ambipolar potential could be achieved by increasing the maximum peak density within the plasma source, either by applying a larger amount of RF power or by increasing the applied magnetic field strength in a helicon plasma source. The production of a double layer structure in the exhaust of a plasma thruster in space, as opposed to the described ambipolar ion acceleration, may require an extra injection of neutral gas in the nozzle region or a secondary downstream cathode (and upstream anode for charge neutrality) to supply a population of electrons in the downstream region of the magnetic nozzle to create and sustain a large amplitude double layer.

In spite of the limitations of the analysis noted above, the calculations presented in this subsection lead us to a significant major conclusion. The result shown in figure 11 provides a clear affirmative validation of the ambipolar acceleration hypothesis.

5. Conclusion

It was possible to describe the plasma potential profiles and the resulting ambipolar ion acceleration observed during the operation of the helicon plasma stage of the VASIMR® VX-200i device, using one-dimensional, magnetized, collisionless, steady-state plasma transport equations with a spatially varying electron temperature. The measured plasma potential was observed to differ from calculated plasma potential values only in the far-plume region of the magnetic nozzle, and agreed closely within the first meter of the magnetic nozzle. A double layer plasma potential-like structure as reported by others was not observed. The peak plasma density and electron temperature within the magnetic nozzle was $1 \times 10^{20}\,\mathrm{m}^{-3}$ and 9 eV, respectively. Within the error bars of measurement, the plasma ionization fraction was 95% to 100% in the magnetic nozzle. The background plasma density and background argon neutral pressure were below $10^{15}\,\mathrm{m}^{-3}$ and 2×10^{-5} Torr, respectively, within the 150 m^3 vacuum chamber during operation of the helicon source. A 20 eV argon ion energy was inferred by plasma potential measurements and directly measured with a retarding potential analyzer (RPA) in the magnetic nozzle. A downstream argon ion velocity of Mach 4 was observed. The recently observed ambipolar ion acceleration would provide added increase in ion velocity during all phases of VASIMR® operation. The result is likely to be an increase in the overall system efficiency of VASIMR®, especially in the high thrust–low I_{sp} operating range.

Acknowledgments

Partial support was provided by the University of Houston Institute for Space Systems Operations (ISSO) Postdoctoral

Fellowship program for B Longmier, formerly an ISSO Postdoctoral Aerospace Fellow.

References

[1] Kash S W 1960 A comparison of ion and plasma propulsion *Proc. IRE* **48** 458–65

[2] Hendel H, Faith T and Hutter E 1965 Plasma acceleration by electron cyclotron resonance *RCA Rev.* **26** 105–21

[3] Sercel J C 1987 Electron-cyclotron-resonance (ECR) plasma acceleration *19th AIAA, Fluid Dynamics, Plasma Dynamics, and Lasers Conf. (Honolulu, HI, 8–10 June 1987)*

[4] Frisbee R H, Blandino J J, Sercel J C, Sargent M S and Gowda N 1990 Advanced propulsion options for the Mars cargo mission *26th AIAA Joint Propulsion Conf. (Orlando, FL, 16–18 July 1990)* AIAA-1990-1997

[5] Hooper E B 1993 Plasma detachment from a magnetic nozzle *J. Propul. Power* **9** 757–63

[6] Stallard B W, Hooper E B and Power J L 1996 Whistler-driven, electron-cyclotron-resonance-heated thruster—experimental status *J. Propul. Power* **12** 814–6

[7] Miller D and Bethke G 1996 Cyclotron resonance thruster design techniques *AIAA J.* **4** 835–40

[8] Gilland J 1998 Helicon sources for electric propulsion *9th Advanced Space Propulsion Workshop (Pasadena, CA, 11–13 March 1998)* pp 607–18

[9] Boswell R W and Chen F F 1997 Helicons—the early years *IEEE Trans. Plasma Sci.* **25** 1229–44

[10] Batishchev O and Molvig K 2001 Kinetic model of a helicon plasma source for VASIMR *AIAA 39th Aerospace Sciences Meeting and Exhibit (Reno, NV, January 2001)*

[11] Boswell R and Charles C 2003 The helicon double layer thruster *28th Int. Electric Propulsion Conf., IEPC 2003 (Toulouse, France, 17–21 March 2003)* Paper IEPC 03-332

[12] Charles C and Boswell R 2003 Current-free double-layer formation in a high density helicon discharge *Appl. Phys. Lett.* **82** 1356

[13] Boswell R W, Sutherland O, Charles C, Squire J P, Chang-Diaz F R, Glover T W, Jacobson V T and Chavers D G 2004 Experimental evidence of parametric decay processes in the variable specific impulse magnetoplasma rocket *Phys. Plasmas* **11** 5125

[14] Charles C and Boswell R 2004 Laboratory evidence of a supersonic ion beam generated by a current-free 'helicon' double-layer *Phys. Plasmas* **11** 1706

[15] Charles C and Boswell R 2004 Time development of a current-free double layer *Phys. Plasmas* **11** 3808

[16] Plihon N, Corr C S and Chabert C S 2005 Double layer formation in the expanding region of an inductively coupled electronegative plasma *Appl. Phys. Lett.* **86** 091501

[17] Plihon N, Corr C S, Chabert C S and Raimbault J-L 2005 Periodic formation and propagation of double layers in the expanding chamber of an inductive discharge operating in Ar/SF_6 mixtures *J. Appl. Phys.* **98** 023306

[18] Sun X, Cohen S A, Scime E E and Miah M 2005 On-axis parallel ion speeds near mechanical and magnetic apertures in a helicon plasma device *Phys. Plasmas* **12** 103509

[19] Sun X, Keesee A M, Biloiu C, Scime E E, Meige A, Charles C and Boswell R W 2005 Observations of ion-beam formation in a current-free double layer *Phys. Rev. Lett.* **95** 025004

[20] Sutherland O, Charles C, Plihon N and Boswell R W 2005 Experimental evidence of a double layer in a large volume helicon reactor *Phys. Rev. Lett.* **95** 205002

[21] Charles C, Boswell R A and Lieberman M A 2006 Xenon ion beam characterization in a helicon double layer thruster *Appl. Phys. Lett.* **89** 261503

[22] Chen F F 2006 Physical mechanism of current-free double layers *Phys. Plasmas* **13** 034502

[23] Lieberman M A, Charles C and Boswell R W 2006 A theory for formation of a low pressure, current-free double layer *J. Phys. D: Appl. Phys.* **39** 3294–304

[24] Charles C 2007 A review of recent laboratory double layer experiments *Plasma Sources Sci. Technol.* **16** R1–R25

[25] Plihon N, Chabert P and Corr C S 2007 Experimental investigation of double layers in expanding plasmas *Phys. Plasmas* **14** 013506

[26] Scime E, Hardin R, Biloiu C, Keesee A M and Sun X 2007 Flow, flow shear and related profiles in helicon plasmas *Phys. Plasmas* **14** 043505

[27] Cox W, Charles C, Boswell R W and Hawkins R 2008 Spatial retarding field energy analyzer measurements downstream of a helicon double layer plasma *Appl. Phys. Lett.* **93** 071505

[28] Goertz C K 1979 Double layers and electrostatic shocks in space *Rev. Geophys. Space Phys.* **17** 418–26

[29] Hershkowitz N 1981 Double layers and electrostatic shocks *J. Geophys. Res.* **86** 3307–10

[30] Hershkowitz N 1985 Review of recent laboratory double layer experiments *Space Sci. Rev.* **41** 351

[31] Hershkowitz N 1989 How Langmuir probes work *Plasma Diagnostics, Discharge Parameters and Chemistry* ed O Auicello and D L Flamm (New York: Academic) pp 114–81

[32] Hershkowitz N 1994 How does the potential get from *A* to *B* in a plasma? *IEEE Trans. Plasma Sci.* **22** 11–21

[33] Fruchtman A 2005 Double layer and thrust *Bull. Am. Phys. Soc.* **50** 109

[34] Fruchtman A 2006 Electric field in a double layer and the imparted momentum *Phys. Rev. Lett.* **96** 065002

[35] Charles C 2005 High source potential upstream of a current-free electric double-layer *Phys. Plasmas* **12** 044508

[36] Aanesland A, Charles C, Lieberman M A and Boswell R W 2006 Upstream ionization instability associated with a current-free double layer *Phys. Rev. Lett.* **97** 075003

[37] Aanesland A, Lieberman M A, Charles C and Boswell R W 2006 Experiments and theory of an upstream ionization instability excited by an accelerated electron beam through a current-free double layer *Phys. Plasmas* **13** 122101

[38] Chang Díaz F R 2003 Progress on the VASIMR engine *39th AIAA/ASME/SAE/ASEE Joint Propulsion Conf. (Huntsville, AL, 2003)*

[39] Bering E A III, Chang Díaz F R, Squire J P, Glover T W, Carter M D, McCaskill G F, Longmier B W, Brukardt M S, Chancery W J and Jacobson V T 2010 Observations of single-pass ion cyclotron heating in a transsonic flowing plasma *Phys. Plasmas* **17** 043509

[40] Arefiev A V and Breizman B N 2008 Ambipolar acceleration of ions in a magnetic nozzle *Phys. Plasmas* **15** 042109

[41] Arefiev A V and Breizman B N 2009 Collisionless plasma expansion into vacuum: two new twists on an old problem *Phys. Plasmas* **16** 055707

[42] Deline C A, Bengtson R D, Breizman B N, Tushentsov M R, Jones J E, Chavers D G, Dobson C C and Schuettpelz B M 2009 Plume detachment from a magnetic nozzle *Phys. Plasmas* **16** 033502

[43] Longmier B W *et al* 2010 VX-200 Performance Results Exceeding 50% Thruster Efficiency, American Institute of Aeronautics and Astronautics *J. Propul. Power, Technical Note* submitted

[44] Biloiu A, Scime E and Biloiu C 2008 Ion beam acceleration in a divergent magnetic field *Appl. Phys. Lett.* **92** 191502

[45] Baalrud S D, Longmier B and Hershkowitz N 2009 Equilibrium states of anodic double layers *Plasma Sources Sci. Technol.* **18**
[46] Gombosi T I 1998 *Physics of the Space Environment* (Cambridge: Cambridge University) pp 187–8
[47] Lieberman M A and Lichtenberg A J 2005 Principles of plasma discharges and material processing *MRS Bull.* **30** 899
[48] Gilland J 2003 Helicon wave physics impacts on electrodeless thruster design *28th Int. Electric Propulsion Conf., IEPC-2003-150 (Toulouse, France, 17–21 March 2003)*